IEEE Access
Multidisciplinary | Rapid Review | Open Access Journal

Received July 23, 2020, accepted August 13, 2020, date of publication August 18, 2020, date of current version August 31, 2020.

Digital Object Identifier 10.1109/ACCESS.2020.3017504

Efficiency Enhancement of a Thermophotovoltaic System Integrated With a Back Surface Reflector

ALI H. KAZIM[1], MOHSINA ASIF[1], KHUJISTA NADEEM[1], ZERTASHA SHOUKAT[1], RABIA NAZIR[2], (Member, IEEE), MUHAMMAD SOHAIL MALIK[3], (Senior Member, IEEE), AND AQSA SHABBIR[4]

[1]Department of Mechanical Engineering, University of Engineering and Technology Lahore, Lahore 54890, Pakistan
[2]Department of Electrical Engineering, University of Engineering and Technology Lahore, Lahore 54890, Pakistan
[3]Department of Mechanical Engineering, Ghulam Ishaq Khan Institute of Engineering Sciences and Technology, Topi 23640, Pakistan
[4]Department of Electrical Engineering, Lahore College for Women University, Lahore 54000, Pakistan

Corresponding author: Aqsa Shabbir (aqsa_shabbir@outlook.com)

ABSTRACT This work aims to investigate the various factors which may affect a thermophotovoltaic (TPV) system's performance, with a special focus on the importance of incorporating a back surface reflector (BSR), which enables below-bandgap photons' recycling. The possible extent to which common PV materials can be used in TPV applications is investigated by comparing them on a Planck distribution curve. The effects of varying BSR reflectivity, TPV cell's external quantum efficiency, and emitter temperature are investigated on the TPV module's efficiency using open-circuit voltage, empirical relations for fill factor, maximum voltage, and photogenerated current. It is shown that TPV applications require materials with smaller (e.g. 0.6 eV $<$ $E_g \leq 0.74$ eV) bandgap energy, e.g. $In_{0.53}Ga_{0.47}As$ (0.74 eV), due to their high percentage of energy ($>$26%) above-bandgap without a spectral control and a small difference between peak and bandgap wavelength. It is shown that the inclusion of a BSR (reflectivity $=$ 1) results in an increase of 15% in TPV efficiency. The results show that by the collective changes of an added BSR, high emitter temperature ($>$2000 K), and improved external quantum efficiency (EQE $\approx$ 1), the present TPV systems can attain efficiency values more than 30% which makes them a favorable prospective choice for Concentrated Solar Power.

INDEX TERMS Back surface reflector, photon recycling, thermophotovoltaic, photovoltaic systems, reflectivity, design optimization, efficiency, solar energy, thermal engineering.

I. INTRODUCTION

In the last decade, a rapid depletion of finite natural resources to meet the increasing energy demands, has worsened the threat of a global energy crisis [1], [2]. Most of the countries are utilizing coal to produce electricity, whereas some are generating electricity by nuclear resources [3] or utilizing water and natural gasses [4] to produce electrical energy. In attempts to avoid an energy crisis propelled by an overconsumption of limited natural resources and to reduce the environmental degradation caused by fossil fuels, there has been an increased interest in employing renewable energy resources as the source of electric power generation [5]–[9]. The best solution to this problem is to replace all non-renewable resources with renewable resources [5]; it has been reported that by 2050, through certain policy alterations, it is possible to meet two-thirds of the global energy demands by using renewable resources [10]. Wind energy and solar energy [11]–[14] are the best examples of renewable energy resources but are currently less reliable than gas or coal due to their dependency on weather conditions. However, increased research and development efforts for renewable energy power generation can help overcome such drawbacks. Recently, *Concentrated Solar Power (CSP)*, in which focused sunlight is used to produce electrical energy [16], has become a subject of discussions. However, it is difficult to harvest photons from the wide solar spectrum and CSP cannot be stored for long time intervals. Thus, to optimally utilize CSP, a system is required that can convert sunlight to an intermediate form of energy and then convert it to electrical energy [17]. *Thermophotovoltaic (TPV)* technology, paired with CSP, is a plausible solution that reduces the area for equipment and utilizes heat energy from a CSP-heated source and converts this heat energy to electricity [18].

The associate editor coordinating the review of this manuscript and approving it for publication was Tarek H.M. EL-Fouly.

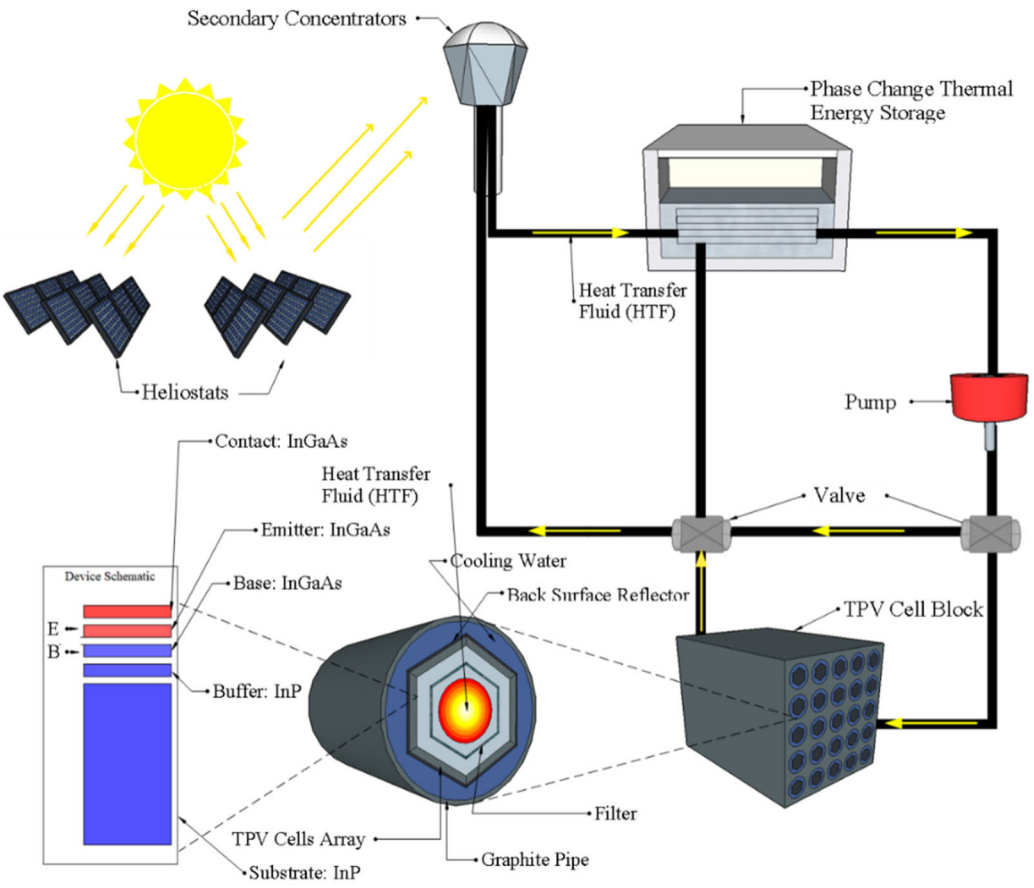

FIGURE 1. TPV incorporated with TES in a CSP-TPV combined power cycle is shown here. Heliostats reflect the solar rays to secondary concentrators. Secondary concentrators charge the HTF (e.g. molten tin, Sn) to be routed to TES where it melts the storage medium (a PCM e.g. silicon, Si). The TPV power cycle consists of graphite pipes acting as emitters enclosed by a hexagonal cavity of the arrays of single-junction TPV cells. For design optimization, filters are placed between the cell and emitter, and BSR is placed behind cells to reflect below and unabsorbed below-bandgap photons, respectively. Cells are water-cooled to maintain a stable temperature at 300 K. The layers of the selected InGaAs cell, constitutes of an InGaAs Contact layer, InGaAs Emitter layer, InGaAs Base layer, InP Buffer layer, and InP Substrate layer of a thickness of 0.025 μm, 0.1 μm, 2.5 μm, 0.3 μm, and 625 μm respectively [15].

In the context of a combined power cycle, a CSP plant based on TPV with a Thermal Energy Storage (TES) is shown in Fig. 1. MATLAB software will be used to simulate the TPV power cycle of the CSP plant and to determine the incident radiations, electrical output, and efficiency of the TPV module. Solar rays are reflected by heliostats and collected by the secondary concentrators. Heat Transfer Fluid (HTF) is pumped to the secondary receiver where its temperature rises through sensible heating. HTF is then taken to TES where it is cooled down. HTF is then further cycled back to the tower to repeat the process. The block diagram in Fig. 2 demonstrates the energy and temperature conversions in the system, where T_{melt} is the temperature of the Phase Change Material (PCM) that has been used and stored within the TES, and T is the temperature of the graphite emitter pipes within the TPV power cycle.

The heat lost from HTF in the TES is used to melt the storage medium, i.e., PCM, within the TES. This enables TES to store thermal energy. Besides storing thermal energy, the TES also maintains the temperature of HTF entering the TPV power cycle. In case of high Partial Shading Condition (PSC) and the temperature of HTF in the secondary concentrators attaining a value below the melting point of the PCM, when HTF will pass through TES the PCM will release energy and heat the HTF. Moreover, flow-diverting valves are also fitted in the system with thermal sensors, that divert low temperature HTF from the TPV power cycle back to TES and secondary concentrators, maintaining constant emissive power conditions for the TPV.

The TPV power cycle consists of pipes with cooling water surrounding the *hexagonal cell cavity,* enclosing the filter, TPV cells, and BSR in a graphite pipe. Graphite pipes are used because they have high emissivity values (> 0.90) [19] and thus, resemble blackbodies in emission properties. A hexagonal cavity is selected because it has the advantage of having a view factor almost equal to 1. The use of a hexagonal cavity within the TPV power cycle, as the closest practically possible configuration to a circular cavity (that has a view

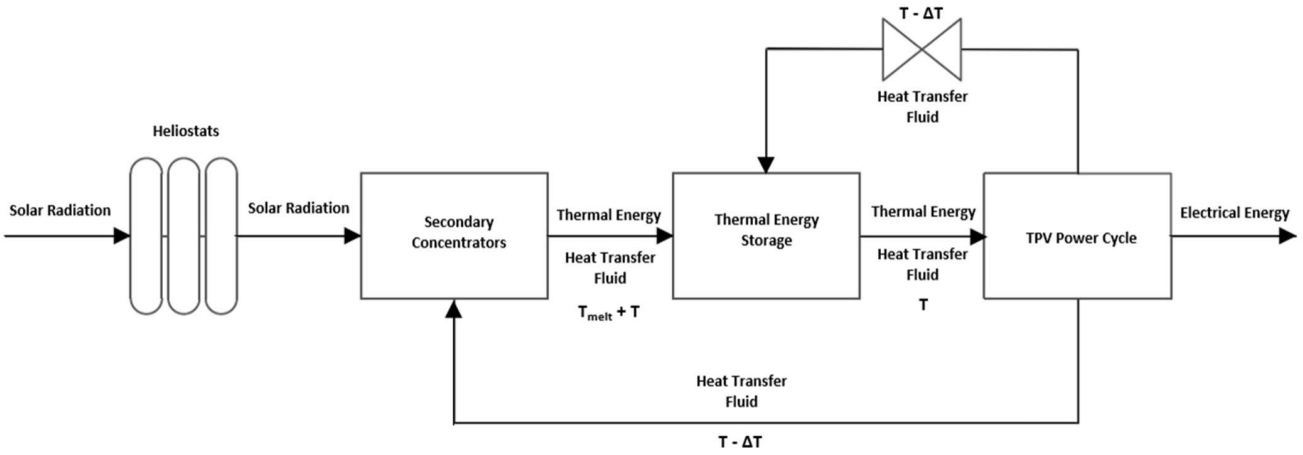

FIGURE 2. The block diagram shows the principle of energy transformation in the discussed configuration of a CSP plant with a TPV power cycle. Sources such as concentrated solar radiations can be used to provide thermal energy to the heat transfer fluid (HTF), heating it to a temperature of $T + T_{melt}$, where T_{melt} is the melting point temperature of the Phase Change Material (PCM) in the thermal energy storage (TES). TES stores thermal energy as PCM is melted, whereas HTF transports thermal energy at temperature T to the TPV power cycle. Within the TPV power cycle, the heated emitter graphite pipes at temperature T convert the thermal energy to radiations, and photons above the bandgap energy are converted into useful electrical energy. HTF, after having been used with the TPV power cycle, to produce electrical energy is at a temperature of $T - \Delta T$, and a part of it is then recycled back to secondary concentrators and the other part to TES through the use of valves. Subsequently, the entire cycle is repeated.

factor = 1 [20]), is distinguished from the existing researches related to CSP and TPV combined systems that instead, utilize flat vertical plates of TPV cells placed between emitter pipes [18]. *Back Surface Reflectors (BSR)* are placed behind every cell array to reflect any unabsorbed photons that are below bandgap to improve efficiency. Moreover, to assist the BSRs, filters are placed between the emitter and cells to reflect any below-bandgap photons. The properties and parameters, of the selected single-junction InGaAs cell, are as recorded by Tuley *et al.* [15]. This cell has a top *contact layer* of InGaAs of thickness 0.025 μm, followed by an *emitter layer* of thickness 0.1 μm. The *base layer* made of InGaAs is 2.5 μm thick and is followed by a *buffer layer* of InP of thickness 0.3 μm. The last layer is the *substrate layer* of InP of 625 μm thickness.

TPV systems generate electricity from the heat by the conversion of radiated photons into charge carriers [21]. TPV systems coupled with solar energy are called Solar Thermophotovoltaic (STPV) systems and have a very high maximum theoretical efficiency exceeding 60% under concentrated light [22], greatly exceeding the Shockley-Queisser limit of 33.7% [23]; making TPV technology one of the most interesting aspects of thermal engineering [24], [25]. The distinguisher between a conventional solar photovoltaic (PV) system and a TPV system is the use of a local emitter (at a temperature mostly lower than 2500 K) in the latter technology instead of the sun as the source of photons, along with the possibility of maximizing the power density by positioning the emitter close to the PV cell [26]. Furthermore, TPV devices due to the emitter being a local source can incorporate different types of *spectral control techniques* (e.g. reflectors and filters). The possible configurations and design optimization of TPV devices, design of cavities, and improved fabrication of TPV cells present TPV devices as systems that have the capability to exceed the conversion efficiencies of conventional solar PV cells [27].

To establish the competitiveness of TPV systems, as a beneficial solid-state engine in a CSP plant, it is important to establish their ability to have an efficiency that is comparable to that of turbines running on Brayton or Rankine Cycles (efficiency = 30%). Recently, a TPV conversion efficiency of 29.1% [28], with the use of reflectors behind the TPV cells, has been recorded. Therefore, the primary focus of this study is to present the conditions needed to achieve an efficiency of the TPV conversion process beyond 30%. The choice of the TPV cell material and the Current-Voltage behavior of the selected TPV cell under given conditions of temperature and radiation wavelengths have a crucial impact on the overall TPV performance.

The novel contributions of this work include the derivation of equations for the determination of maximum voltage with the use of certain equations and empirical relations that reduce the computational efforts and the need of extensive experimentation and measurements, and the investigation of the impact of more than one factor (BSR, EQE, and emitter temperature) on the efficiency of TPV module. The maximum current and peak voltage can be calculated for any emitter temperature using only the experimental EQE values and dark I-V curve, both of which are, mostly, provided by the PV cell manufacturer. The rest of the paper is structured as follows. Section II outlines the materials used for TPV cells, losses in a TPV system, and the significance of back surface

reflectors. Section III presents the methodology, followed by Section IV that outlines the results and accompanying discussion. Section V concludes the paper.

II. THERMOPHOTOVOLTAIC SYSTEMS

A. MATERIALS USED FOR TPV CELLS

A photovoltaic cell, the most integral part of any TPV system, is manufactured with a variety of special materials named as semiconductors. Most of the used cells are single-junction cells but multijunction cells (having a range of bandgap wavelengths) can also be used for the TPV system [29]. The TPV cells that are compared in this paper are as follows [20]:

- Silicon (Si)
- Germanium (Ge)
- Silicon-Germanium (SiGe)
- Gallium Antimonide (GaSb)
- Indium Gallium Arsenide (InGaAs)
- Indium Gallium Arsenide Antimonide (InGaAsSb)
- Gallium Arsenide (GaAs)
- Cadmium Telluride (CdTe)

Silicon (Si) has a uniform single-crystal structure and belongs to the IV group. To make a perfect PV cell, Si may be doped with other semiconductors. Using Si PV cells, many TPV prototypes have been developed, with the foremost developed TPV model also being based on a Si PV cell [30]. Si has a bandgap energy E_g of 1.12 eV at a temperature of 300 K. Germanium (Ge) cells show poor performance and are mostly used in multijunction solar converters as bottom cells. Ge has a bandgap energy of 0.66 eV and their efficiency of conversion is 6.7%. It has been noticed that high voltage factor is one of the major challenges of Ge PV cells and BSRs for these cells are normally feasible. Silicon germanium (SiGe) alloys can have different bandgap energies between the range of 0.66 eV and 1.12 eV. The bandgap energy of SiGe can be altered by changing the composition of the cell [31]. Gallium Antimonide (GaSb) has a bandgap energy of 0.72 eV, has proved to be one of the best choices for TPV generators [32], and mostly acts as bottom cells for tandem solar PV converters. GaSb PV cells have a poor efficiency of 3% but show improvement of up to 18.5% by using BSRs. The bandgap energy of Indium Gallium Arsenide, ($In_xGa_{1-x}As$) can be varied from 0 to 1 by changing x. Lower bandgap lattice-mismatched InGaAs cells are gaining increased interest in the conversion of light energy into electrical energy [33]. Indium Gallium Arsenide Antimonide (InGaAsSb) gives two degrees of freedom in tuning both lattice constant and bandgap [20] and has an average 0.52 eV bandgap energy. Gallium Arsenide (GaAs) has high absorptivity and can absorb light with the thickness of a few microns. GaAs cells are not affected by heat and show resistance to radiation that can cause damage, so they are highly appreciated in space applications. Cadmium Telluride (CdTe) has very high absorptivity and is also a cost-effective material.

B. LOSSES IN A TPV SYSTEM

The performance of a TPV system may be diminished due to several losses, broadly classified as fundamental and practical losses [18]. The practical losses, discussed here, can be reduced by improving the design and fabrication of the components of the TPV system. These losses consist of the optical losses [34] such as the *thermalization losses* due to the bandgap energy being considerably smaller than the energy in emission spectrum [35]; *non-absorption losses*, due to the proportion of emission spectrum, reported to have an average value of 55% [36], having energy below the bandgap energy of cell; *reflection losses*, due to the photons being reflected from the top-most layer of TPV cell and not being reabsorbed by the emitter due to a large emitter-cell distance; and *transmission losses* due to absorption in the TPV cell's layers thicknesses [37], [38]. Moreover, there are also radiative losses such as the emitter-to-cell loss caused due to the cell and emitter not being placed close enough and having a view factor below 1 [39]. Other losses such as *radiative recombination losses,* when the separated charge carriers recombine to release a photon, and *non-radiative recombination losses,* when the recombination results in phonon generation instead of a photon, are dependent on the cell material [40].

C. SPECTRAL CONTROL: BACK SURFACE REFLECTOR

To minimize the aforementioned losses, it is important to select a TPV cell that: has its bandgap wavelength closely matched to the peak wavelength and blackbody spectrum of the emitter, is positioned close to the emitter with minimum edge effects and a view factor of nearly 1, and is paired with a *spectral control technique*. Selective emitters are a type of this technique that suppress the emissions of below-bandgap radiations by having a variable emissivity for different wavelengths [41]. However, there have been limitations regarding the identification of a *selective emitter* material that performs effective suppression and is easy to manufacture along with being cost-effective because most of these emitters are made of integrated photonic crystals or oxides containing rare-earth metals [42]–[45]. *Filters*, another method of spectral control, are placed between the emitter and cell and can be used to either reflect below-bandgap photons or offer very low absorption for above-bandgap photons albeit imperfectly [46]. *Back Surface Reflector (BSR),* the spectral control technique focused upon in this paper, is placed behind the TPV cell to reflect photons, that are below bandgap and not absorbed by the cell, to the emitter. BSRs have proved to be a very useful technique for photon recycling [29] and are simple to incorporate as a mirror [28] or an element with high reflectivity in the infrared region, such as gold (Au) or silver (Ag) [18], [47], can be used as a BSR.

III. METHODOLOGY

In this paper, a TPV system for its potential application within a CSP system has been modeled and some of the factors

that can significantly affect its performance have been determined. The TPV system can be placed within a CSP plant as the core electricity generation system, where central pipes, carrying HTF, function as the emitter and the temperature of the fluid is maintained using a TES tank [18]. The pipes are envisioned to be made of graphite [48], due to its low chemical reactivity, high emissivity value ($\varepsilon = 0.91$ [49]), and low cost.

A. CHARACTERIZATION AND SELECTION OF TPV CELL MATERIAL

The emissions from the graphite emitter are modeled using the Planck distribution function for blackbodies [22], with the imperfection in emissions accounted for by the inclusion of ε in the function. Thus, the emissive power E in W/m^2 within a certain wavelength λ band is given by [50]:

$$E(\lambda, T) = \int_{\lambda_1}^{\lambda_2} \frac{\varepsilon \times C_1}{\lambda^5 \left[e^{\left(\frac{C_2}{\lambda T}\right)} - 1 \right]} d\lambda \tag{1}$$

In the previous equation, $C_1 = 3.742 \times 108$ W/m$^2\mu$m^{-4} and $C_2 = 1.4388 \times 10^4$ Kμm and T is the temperature of the emitter in Kelvin.

The peak wavelength λ_p at which the emissive spectral distribution has its maximum value, is given by the Wein's displacement law [51]:

$$\lambda_P \times T = 2898 \mu m.K \tag{2}$$

The above relation establishes an inverse relationship between the peak wavelength and the emitter temperature. For the good performance of TPV cells, the cell must preferably have a bandgap wavelength λ_g slightly longer than the peak wavelength λ_p because, in case of λ_p being very short as compared to λ_g, there are excessive thermalization losses in the cell. The bandgap wavelength λ_g of a TPV cell can be found using its bandgap energy E_g in eV [52]:

$$\lambda_g = \frac{hc}{E_g q} \tag{3}$$

h is the Planck's constant, c is the speed of light, and q is the charge of one electron in Coulombs. The portion of the spectrum that is useful for a TPV cell, is the above-bandgap region that has photons having wavelengths shorter than λ_g. This proportion of above-bandgap photons in any emission spectrum, for an emitter and TPV cell material combination, is given by the percentage energy above-bandgap $\eta_{E>Eg}$ [53]:

$$\eta_{E>Eg} = \frac{E_{(\lambda_{min} \to \lambda_g)}}{E_{b_{(0 \to \infty)}}} \times 100\% \tag{4}$$

The total emitted spectral power, $E_{b(0\to\infty)}$ can be calculated using the following equation, where σ is the Stefan-Boltzman constant [50]:

$$E_{b_{(0\to\infty)}} = \int_0^{\infty} \frac{\varepsilon \times C_1}{\lambda^5 \left[e^{\left(\frac{C_2}{\lambda T}\right)} - 1 \right]} d\lambda = \varepsilon \sigma T^4 \tag{5}$$

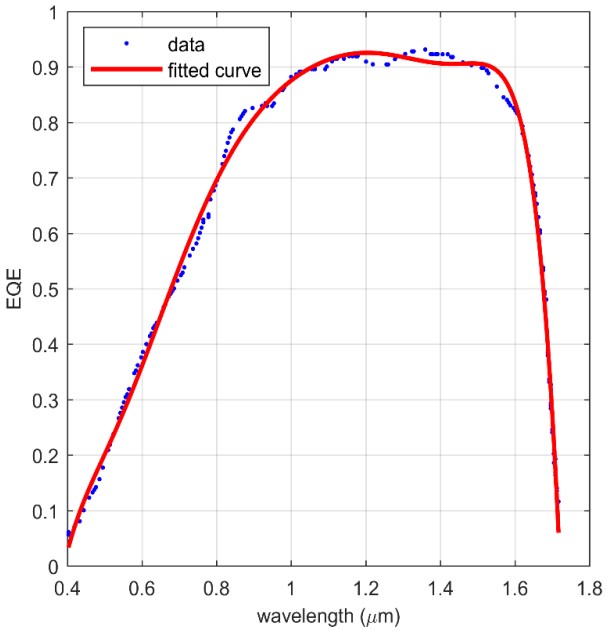

FIGURE 3. Experimentally measured data [15] and curve of best fit for EQE for a typical 0.25 cm^2 n-p InGaAs TPV cell.

B. VOLTAGE-CURRENT AND EFFICIENCY CHARACTERIZATION OF TPV SYSTEM

1) EXTERNAL QUANTUM EFFICIENCY

External Quantum Efficiency (EQE) is a measure of the probability that a photon incident on a TPV cell will be absorbed by the TPV cell and result in the generation of charge carriers [54]; the EQE of the photons with energy below the bandgap energy is zero.

Ideally, each absorbed above-bandgap photons must generate at least one hole-electron pair. However, in actuality, some pairs of charge carriers (the holes and electron) may recombine after separation before reaching the external circuit, and upon recombination release a photon (radiative recombination) [55] or phonon (non-radiative recombination). EQE is a characteristic of the TPV device only, without depending on the properties of the emitter [56]. Ideally, EQE must be constant and equal to 1 for all wavelengths, however, due to recombination losses, it shows an irregular pattern for different photon wavelengths.

Different cell materials have different distributions of EQE that can be measured by experiments or are provided in the specifications of the TPV cell by the manufacturer [57], and the procedure described here can be used for any cell material's data. For example, the practical values of EQE for a 0.25 cm^2 n-p InGaAs cell can be obtained by producing a curve, as shown in Fig. 3, using the experimental data measured by Tuley *et al.* [15].

The fitted curve, from Fig. 3, for the EQE of the n-p InGaAs TPV cell has the following polynomial equation:

$$\begin{aligned} EQE(\lambda) = {} & -55\lambda^8 + 441.46\lambda^7 - 0.0015\lambda^6 + 0.0029\lambda^5 \\ & - 0.0034\lambda^4 + 0.0025\lambda^3 - 0.0011\lambda^2 + 260.91\lambda \\ & - 26.89 \end{aligned} \tag{6}$$

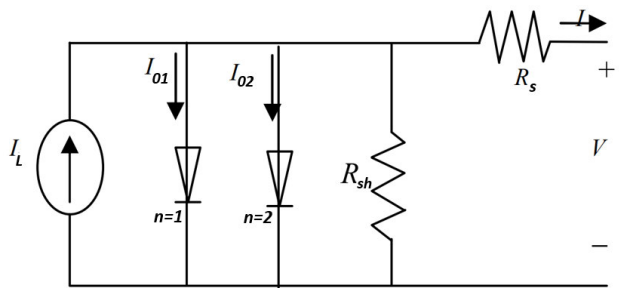

FIGURE 4. The 2-Diode Model used to represent the electricity generation in a *real* TPV cell as the effects of series resistance R_s and shunt resistance R_{sh} are included. I_{01} and I_{02} are the dark saturation currents of the two diodes and I_L is the photocurrent.

The average EQE, $\overline{EQE}$, for the wavelength equal to or shorter than the bandgap wavelength is calculated by:

$$\overline{EQE} = \frac{1}{\lambda_g - \lambda_{min}} \left(\int_{\lambda_{min}}^{\lambda_g} EQE\,(\lambda)\,.d\lambda \right) \tag{7}$$

where λ_{min} is the smallest wavelength for which the EQE is recorded. The calculated $\overline{EQE}$ is 0.7097 for the n-p InGaAs TPV cell.

2) DOUBLE DIODE MODEL

A double diode model is the equivalent circuit model which is used here to define the voltage-current behavior of the TPV cell as it presents greater accuracy than a single diode model [58], with the second diode representing the recombination losses in the depletion region [59].

Fig. 4 shows the circuit diagram of the double diode model, used to define the electrical parameters of the TPV cell.

Therefore, the current-voltage characteristics of the cell are given by [60]:

$$I = I_L - I_{01}\left(e^{\frac{q(V+IR_s)}{n_1 kT_c}} - 1\right) - I_{02}\left(e^{\frac{q(V+IR_s)}{n_2 kT_c}} - 1\right) - \frac{V + IR_s}{R_{sh}} \tag{8}$$

I_L is the photocurrent in Amperes (A); I_{01} and I_{02} are the anti-parallel ideal saturation currents (in A) of the first and second diode, respectively; n_1 is the ideality factor of the first diode and is assumed to be equal to 1 [61]; n_2 is the ideality factor of the second diode and is assumed to be equal to 2 [62], T_C is the cell temperature (in Kelvin); k is the Boltzmann constant; R_S is the series resistance; and R_{sh} is the shunt resistance (in ohm). An efficient TPV cell will have a very high R_{sh} and a low R_s.

For simplification purposes, -1 is ignored in both the second and third term of (8) [63]. It is also assumed that both the photons' level of injection and the quality of cell fabrication are very high resulting in a very large value of R_{sh} (almost infinity). Thus, the last term in (8) is neglected, simplifying the equation to:

$$I = I_L - I_{01}\left(exp^{\frac{q(V+IR_s)}{kT_c}}\right) - I_{02}\left(exp^{\frac{q(V+IR_s)}{2kT_c}}\right) \tag{9}$$

3) THE V-I CHARACTERISTICS

To calculate I_L, the number of photons having energy equal to or greater than the bandgap energy emitted from the emitter source per unit area, i.e., the useful photon flux φ ($m^{-2}s^{-1}$) needs to be determined first [64]:

$$\varphi(/m^2 s) = \frac{E_{(\lambda_{min}\to\lambda_g)}}{\left(\frac{1}{(\lambda_{min}+\lambda_g)(10^{-6})}\right)\left(\int_{\lambda_{min}\times 10^{-6}}^{\lambda_g\times 10^{-6}} \frac{hc}{\lambda} d\lambda\right)} \tag{10}$$

The denominator in (10) represents the average energy of photons, in Joules, for the emitter's range of wavelength from λ_{min} to λ_g.

The photocurrent I_L, i.e., the amount of electric current generated when the TPV cell is illuminated is calculated by [20]:

$$I_L = Area\ of\ module \times q \times \varphi \times \overline{EQE} \tag{11}$$

The dark saturation currents, I_{01} and I_{02}, can be determined by substituting $I_L = 0$ in (9), changing the equation to:

$$I = I_{01}\left(e^{\frac{q(V+IR_s)}{kT_c}}\right) + I_{02}\left(e^{\frac{q(V+IR_s)}{2kT_c}}\right) \tag{12}$$

Solving (12) simultaneously, using two sets of measured voltage and current values in dark conditions, the dark saturation currents can be found.

For example, for the 0.25cm^2 InGaAs cell, I_{01} and I_{02} can be found using experimentally recorded value of R_s (R_s = 0.25 mΩcm^2) and a set of random values from experimental data recorded in dark conditions [15], as shown in Fig. 5. The accuracy of this model, used to find I_{01} and I_{02}, can be further improved by experimentally validating the value of R_{sh} before eliminating the last term of (8).

The open circuit voltage V_{OC}, i.e., the potential difference across the external circuit when the net current through the external circuit is zero, is found by modifying (9) as [65]:

$$I_L = I_{01}\left(e^{\frac{q(V_{OC})}{kT_c}}\right) - I_{02}\left(e^{\frac{q(V_{OC})}{2kT_c}}\right) \tag{13}$$

A TPV module's fill factor η_{FF} is the ratio of the product of maximum voltage V_m, and maximum current I_m to the product of I_L and V_{OC}. Realistically, the fill factor is less than 1.

V_m is mostly determined by experimentation [66], however, in case of the absence of an experimental setup and data for a TPV system, the novel alternative technique adopted here can be used for its evaluation. Here, to find V_m, two empirical relations for fill factor η_{FF}— the theoretical limit of η_{FF} given by Green $\eta_{FF,Green}$ [67] and the theoretical limit of η_{FF} given by Shockley and Queisser $\eta_{FF,Shockley}$ [55], have been used. Except for a small range of very low V_{OC} values, both empirical relations result in equivalent fill factor values, as has been demonstrated in [20].

The empirical relations for the theoretical limits of η_{FF}, as derived by Green and Shockley, are as follows [20]:

$$\eta_{FF,Green} = \frac{\frac{V_{OC}}{V_c} - \ln\left(\frac{V_{OC}}{V_c} + 0.72\right)}{\frac{V_{OC}}{V_c} + 1} \tag{14}$$

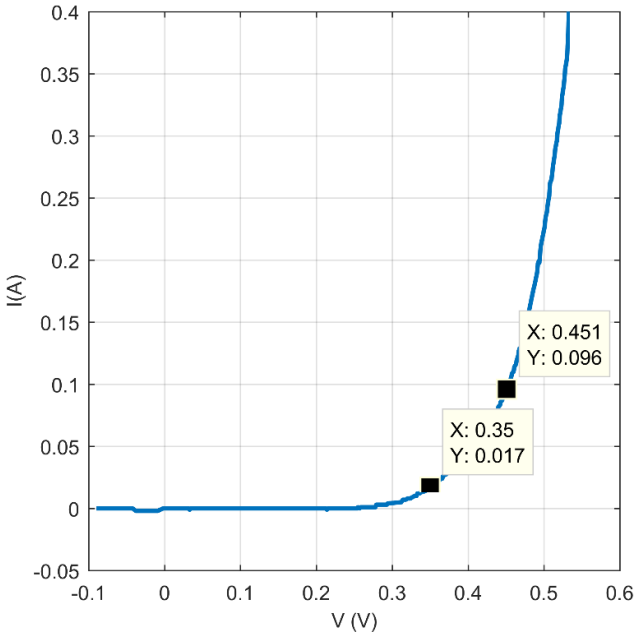

FIGURE 5. Experimental [15] I-V curve of an n-p InGaAs TPV cell at 30°C under dark conditions, showing how an experimental dark I-V curve can be used to determine dark saturation currents, I_{01} and I_{02}. The two data sets used in this work are (0.35, 0.017) and (0.451, 0.096).

In the above equation, V_c is thermal voltage given by [20]:

$$V_c = \frac{kT_{cell}}{q} \tag{15}$$

$$\eta_{FF,Shockley} = \frac{\left(\frac{V_m}{V_c}\right)^2}{\left(1 + \frac{V_m}{V_c} - e^{-\frac{V_m}{V_c}}\right) \times \frac{V_{OC}}{V_c}} \tag{16}$$

To find V_m, (14) and (16) are equated and solved for the unknown, V_m.

4) EFFICIENCY OF THE TPV SYSTEM

The net efficiency of the TPV module, with a BSR with reflectivity R, is determined using the following equation [49]:

$$\eta = \frac{I_L \times V_m}{\int_{\lambda_{min}}^{\infty} \frac{\varepsilon \times C_1}{\lambda^5\left[\exp\left(\frac{C_2}{\lambda T}\right)-1\right]} d\lambda - R\int_{\lambda_g}^{\infty} \frac{\varepsilon \times C_1}{\lambda^5\left[\exp\left(\frac{C_2}{\lambda T}\right)-1\right]} d\lambda} \tag{17}$$

As evident from the previous equation, the inclusion of a BSR by reflecting and recycling the below-bandgap photons, decreases the value of the effective total input energy, and increases the net efficiency, in contrast to the absence of any BSR.

IV. RESULTS AND DISCUSSION

The choice of an appropriate material for the TPV cell is of utmost importance. Here, 8 different PV cells will be analyzed as single-junction cells based on their behavior with the distribution of spectral emissive power for a typical emitter temperature of 1750 K. Each material's bandgap energy E_g, the proportion of useful region of the emissive spectrum that is above bandgap $\eta_{E>Eg}$, and the difference of bandgap wavelength λ_g and peak wavelength λ_p are compared through tabulated and graphical means.

TABLE 1. 8 PV cell materials that are compared for selection in a TPV application. Bandgap energy E_g and bandgap wavelength λ_g are measured at 300 K [20]; the peak wavelength λ_p and percentage energy above bandgap $\eta_{E>Eg}$ is for an emitter at 1750 K.

Materials	E_g (eV)	λ_g (μm)	λ_g - λ_p (μm)	$\eta_{E>Eg}$ (%)
InGaAsSb	0.55	2.25	0.60	48.06
Ge	0.66	1.88	0.22	34.43
GaSb	0.72	1.72	0.07	28.17
InGaAs	0.74	1.68	0.02	26.31
CIS	1.00	1.24	-0.42	9.71
Si	1.12	1.11	-0.55	5.83
CdTe	1.50	0.83	-0.83	1.01
CGS	1.70	0.73	-0.93	0.38

Using the selected cell material, a complete system is designed where a TPV block is used as the conversion system of a CSP plant. For the selected cell material, the useful above-bandgap emissive power is quantified and used to determine the photon flux. Voltage, current, and all related performance parameters are then evaluated for a real TPV module, characterized based on a realistic case, with an experimental average value of EQE and then for an ideal TPV module that has EQE equal to 1. The conversion efficiency is evaluated for both ideal and real TPV modules at an average emitter temperature of 1750 K and at a range of emitter temperatures. The extent to which these variable factors impact the overall efficiency of TPV power generation is investigated.

A. SELECTION OF A TPV CELL MATERIAL

In Table 1, the various available choices of PV cell materials are compared based on their bandgap wavelength λ_g, percentage energy above-bandgap $\eta_{E>Eg}$, and relation with peak wavelength λ_p for an average emitter temperature of 1750 K. It has been concluded by Lenert *et al.* [68] that when selecting an optimum TPV cell, its bandgap wavelength must be matched with the peak wavelength of the emitter. At 1750 K, the λ_p is calculated using the Wein's Displacement law (2) and determined to be 1.656 μm.

In the ensuing analysis, it is assumed that the TPV cells are water-cooled, with the cell temperature remaining constant at 300 K, as the bandgap of a cell is a function of temperature.

Each material's bandgap energy, the useful region of emissive power above-bandgap, and the difference of bandgap wavelength and peak wavelength are compared in Fig. 6.

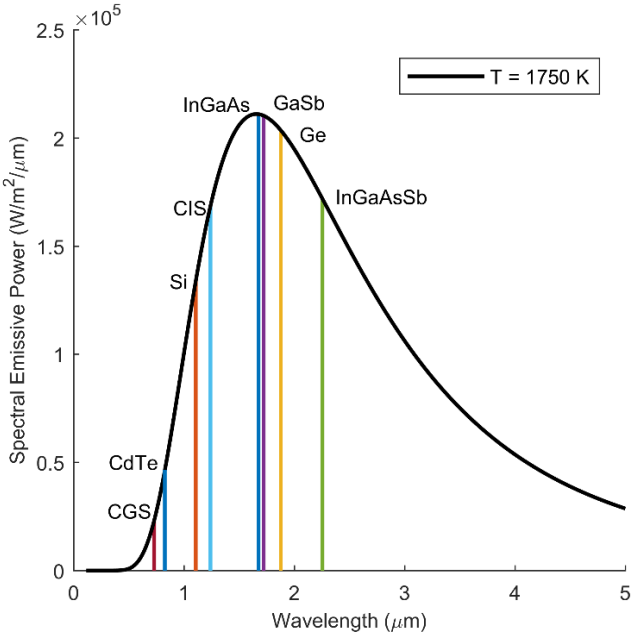

FIGURE 6. A distribution of spectral emissive power (W/m^2/μm) against Wavelength (μm) at an average emitter temperature of 1750 K with a peak wavelength of 1.656 μm and a comparison of the bandgap wavelengths, λ_g of 8 different PV cell materials on this distribution curve. CGS, a high bandgap cell, has the shortest λ_g (0.729 μm) and above bandgap photons' region, whereas, InGaAsSb, a low bandgap cell, has the longest λ_g (2.254 μm) and the largest above-bandgap region.

Fig. 6 compares these materials with respect to the Planck's distribution curve for a constant temperature of the TPV emitter source. Moreover, in this comparison, the irradiance is considered to be uniform (100%) as the analysis is only conducted for a single TPV cell instead of an array, and therefore, does not have mismatch losses. As can be observed from Fig. 6, the high bandgap cells, such as CGS and CdTe due to to their very short bandgap wavelengths, are presented with a negligible useful area above the bandgap energy for a blackbody emitter temperature at 1750 K ($\eta_{E>Eg}$ is equal to 0.377% and 1.01% respectively, Table 1). PV cells made of Si ($E_g = 1.10$ ev) are the most widely used type in the solar PV modules [69], however, as is evident from Fig. 6, the useful region for its bandgap wavelength is towards the left of peak wavelength and is not sufficiently large, i.e., $\eta_{E>Eg} =$ 5.830%. The behaviour of CIS closely corresponds to that of Si. Conversely, InGaAsSb ($E_g = 0.55$eV) has the smallest bandgap energy, thus, the least amount of energy is required to be absorbed by the InGaAsSb cell to generate electron-hole pairs. However, the peak wavelength is shorter than the bandgap wavelength of InGaAsSb ($\lambda_g - \lambda_p = 0.6$ μm) and without a spectral control, this excessive and intense above bandgap energy will result in overheating of the PV cell and thermalization losses.

The bandgap wavelengths of Ge, GaSb, and InGaAs have a small difference with the peak wavelength of a blackbody emitter at 1750 K (the difference, λ_g - λ_p, is 0.2μm, 0.07μm, 0.02 μm, respectively) and the percentage area above bandgap, $\eta_{E>Eg}$ is also within an acceptable range (34.428%, 28.17%, and 26.31%, respectively). Moreover, these PV cells that have $E_g > 0.6$ eV require a lower suppression of Auger recombination and low series resistance leading to a better TPV cell performance [70]. GaSb and InGaAs cells have an advantage, compared to Ge (a single element), of the possibility of tuning their bandgap energies by changing the composition of their constituent elements. With increasing number of materials, i.e., ternary and quaternary PV cells, the range of useful photons has been observed to increase with specific compositions. This leads to an increased electrical power density even at lower emitter temperatures, thus increasing the efficiency [71]. GaAs and InP substrates are considered to be the most optimum choice for PV cells. However, trends have been shifting towards lower frequency substrates such as InP. The purpose of selecting InP substrate was to contribute in overcoming the low efficiency challenges as TPV cells grown on these substrates are potentially more efficient. Therefore, $In_{0.53}Ga_{0.47}As$ TPV cells grown on InP substrates, due to the reasons stated above, the availability of sufficient experimental measurements related to it in literature (as used in the ensuing analysis), and widespread use in TPV applications, particularly those pertaining to CSP, is selected for further analysis [18], [48].

B. EFFICIENCY OF A REAL (EQE ≠ 1) TPV MODULE

In the TPV system, $In_{0.53}Ga_{0.47}As$ cells grown on reusable InP substrates are used. The region of the emitter's spectral distribution that has energy above the bandgap energy of the InGaAs ($E_g = 0.74$eV) is the useful portion for the electricity generation process. For an average arbitrary temperature of 1750 K, the area is as shown in Fig. 7.

For the real case, the average experimental external quantum efficiency $\overline{EQE}$ is evaluated using (7) and Fig. 3; found to be equal to 0.7097. The photocurrent density I_{ph} is equal to 5.791 A/cm^2. The photocurrent I_L is calculated using (11), where the total number of photons incident on the TPV cell is used. For an area of module equal to 0.25 cm^2, I_L is 1.4475 A.

To evaluate the ideal dark saturation currents I_{01} and I_{02}, (12) and Fig. 5 are used; $I_{01} = 3.2218 \times 10^{-9}$A and $I_{02} = 1.8320 \times 10^{-9}$ A. The effect of series resistance R_s is included by using an average value of 0.25 mΩ.cm^2 for an InGaAs cell, as experimentally measured by [15]. Furthermore, (13) - (16) are used to calculate V_{oc}, found to be equal to 0.5133 V, and V_m, which is equal to 0.4382 V in this case. The effect of BSR reflectivity R on the TPV module's efficiency η is investigated, by using the formula in (17). The relation between η and R is shown in Fig. 8.

As observed in Fig. 8, the module's net efficiency η (%), shows an exponential increase with increasing BSR's reflectivity R. With no BSR ($R = 0$), the efficiency is very low ($\cong$ 5.5%), whereas, when a perfect BSR ($R = 1$) is incorporated behind the TPV module, it reflects all of the photons with energy below bandgap to the emitter and the efficiency attains a value of 20%.

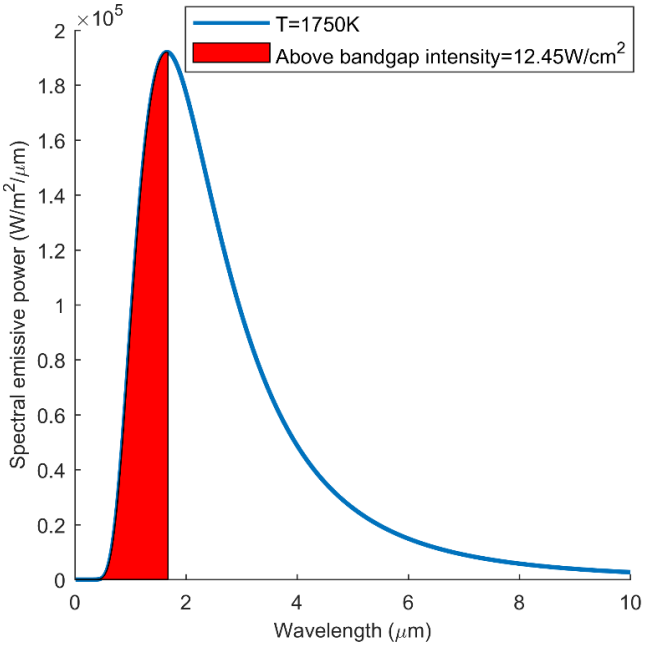

FIGURE 7. The blue curve shows the spectral emissive power distribution, derived from Planck distribution, for a graphite emitter at a temperature of 1750 K, and $\varepsilon = 0.91$. The red shaded region is the emissive intensity, having energy above the bandgap energy (0.74 eV) for an InGaAs TPV cell.

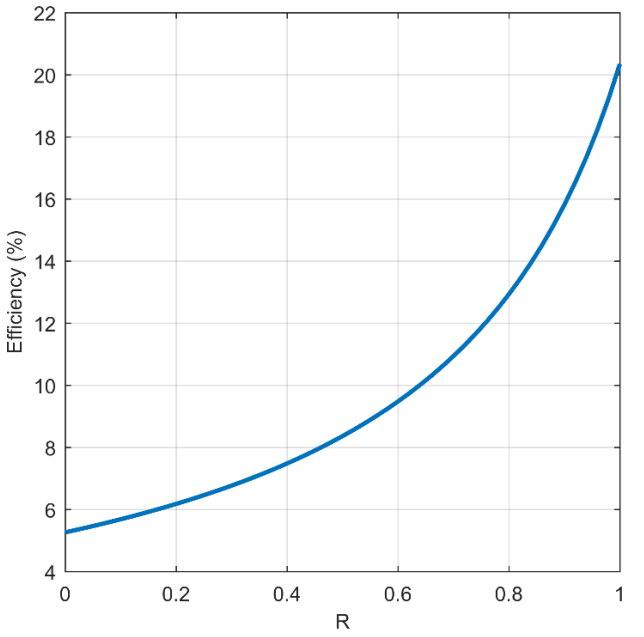

FIGURE 8. Efficiency, η (%) of a real 0.25 cm^2 InGaAs module ($\overline{EQE}$ = 0.7097) with respect to BSR reflectivity R for an emitter temperature T of 1750 K. Increasing R also increases the module's η.

C. EFFECT OF BLACKBODY EMITTER TEMPERATURE ON EFFICIENCY OF TPV MODULE (EQE≠1)

When the emitter temperature in a TPV system is increased, the total spectral emissive power also increases leading to a greater above-bandgap photon flux, and larger photogenerated current. The effect of increasing emitter temperature is

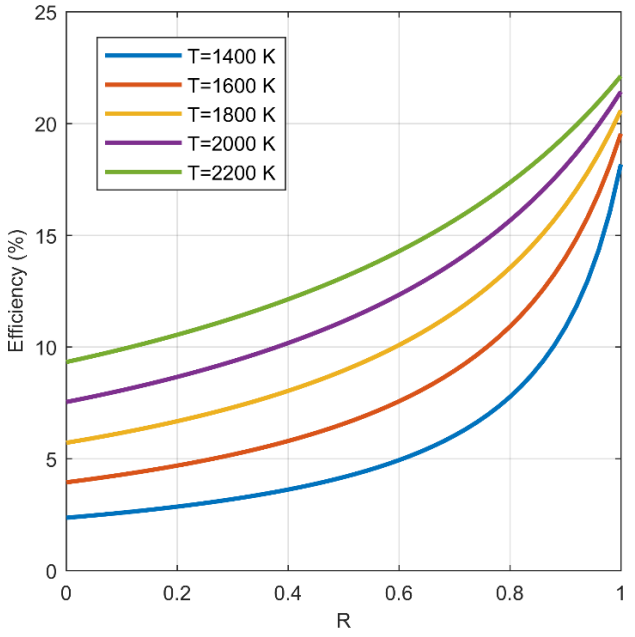

FIGURE 9. Effect of varying emitter temperature on the TPV efficiency, η (%) with BSR reflectivity R for a 0.25 cm^2 TPV module with $\overline{EQE} = 0.7071$ (EQE $\neq$ 1). Increasing the emitter's temperature T increases TPV conversion efficiency.

investigated by iterating the emissive power and efficiency values for different emitter temperatures. The impact of emitter temperature on the efficiency of the TPV module is shown in Fig. 9.

As the emitter temperature T is increased, the performance of the TPV module also improves, as shown by the increase in TPV conversion efficiency. With no BSR, as T is increased from 1400 K to 2200 K, η steadily increased from 2.36% to 9.36%, whereas at $R = 1$, this increase is smaller and is from 18.2% to 22.16%.

D. COMPARISON OF THE EFFICIENCY OF AN IDEAL (EQE = 1) TPV MODULE WITH A REAL (EQE ≠ 1) TPV MODULE

To evaluate the extent to which improvements in the TPV module's technology is possible, an ideal case has also been investigated, where the EQE is assumed equal to 1, i.e., all the incident photons on each TPV cell will generate an equivalent proportion of charge carriers that will be collected by the TPV cell's external circuit. It has been identified that increasing the intensity of the emitter can increase EQE [72], using a PV cell material with higher absorption coefficient (e.g. perovskite) [73], better anti-reflection coating and front surface texturing [74], using multijunction cells that combine sub-cell materials such that each sub-cell's range of wavelengths for high EQE is offset from the other so the net effect is a high EQE through a wider spectrum of emitter radiation's wavelength [75], and low bandgap cells made of quantum nanostructures [76] can improve EQE.

For the ideal case, the dark saturation currents (I_{01} and I_{02}) are the same as those calculated for the real case;

TABLE 2. The efficiency enhancement achieved in this paper, using back surface reflector (BSR) behind the TPV cell, an external quantum efficiency (EQE) of 1, and increasing the emitter temperature are compared to efficiency enhancement techniques investigated in other case studies. The other techniques mentioned here include the use of multijunction cells, high performance selective emitter, and different configurations of TPV cells with respect to the emitter.

	Description [20]	Working [20]	Case Study
Temperature of emitter	Emitter in TPV system is used to radiate the thermal radiations that will be absorbed by the TPV cell.	It is located before the PV cell in TPV system. By increasing the temperature, efficiency of TPV system also increases.	In this paper, it is found that for a real (EQE < 1) PV cell, emitter temperature must be greater than 1800 K to have an $\eta > 20\%$. At $R = 1$, as temperature is increased from 1400 K to 2200 K, η increased from 18.2% to 22.16%.
Back surface reflector (BSR)	Back surface reflector is a spectral control technique used to improve the efficiency of TPV system.	It is located behind the TPV cell and reflects all the unused photons so that they can be used again.	In this paper, it is concluded that if only a BSR (with $R = 1$) is used as an optimization technique in TPV system then the efficiency can be increased by 15% for an InGaAs cell, attaining an efficiency of ~19% at 1600 K.
External Quantum Efficiency (EQE)	EQE is the most representative performance indicator quantity of a PV cell that shows the probability that photons, upon striking the PV cell, will be converted to electrical energy.	Using a TPV cell with good surface reflectivity, front surface texturing, and high absorption coefficient can enhance the EQE of the system.	In this paper, at an emitter temperature of 1600 K and R of 1, at EQE $\neq$ 1 (i.e., EQE = 0.7071), the efficiency is 19.57%, whereas at EQE =1 this efficiency is 28.18%.
Multijunction cells	Multijunction cells are those cells that have different semiconductors and multiple p-n junctions.	Multijunction cells, unlike single junction cells, are composed of multiple bandgaps and can therefore, utilize multiple wavelengths of the radiation spectrum.	Datas [29] mathematically modeled a TPV system, that at an emitter temperature of 1600 K with no BSR, demonstrated maximized efficiency of 26.5% for single junction cells and 36.7% for multijunction cells.
High Performance Selective Emitters	Selective emitters are often used to adapt the spectrum of incident light on the PV cell, stopping any unwanted light that may lead to cell heating or recombination.	Selective emitters located before the TPV cells only direct the above band gap photons to cell and in this way output of the system increases but input decreases, leading to high efficiency of the system.	Pfiester et al. [22] found that a system consisting of a photocell, absorber, and thermally selective emitter have an efficiency of 8% at 1640 K. But the cost of selective emitter is another factor that limits its use.
TPV cell configurations	The most common cell configurations are planar and cylindrical designs. Cylindrical cavity arrangements are the best for improving the efficiency of system.	A cavity consisting of a cylindrical TPV cell and emitter in its inner side and mirror on its outside is one of the best choices of TPV system. It has lesser thermal losses as compared to other configurations, e.g. planar, where the unabsorbed photons are wasted even if the system has a BSR.	Khvostikov et al. [77] experimentally determined an efficiency of 4.5% when a cylindrical cavity and GaSb cell were used in a STPV.

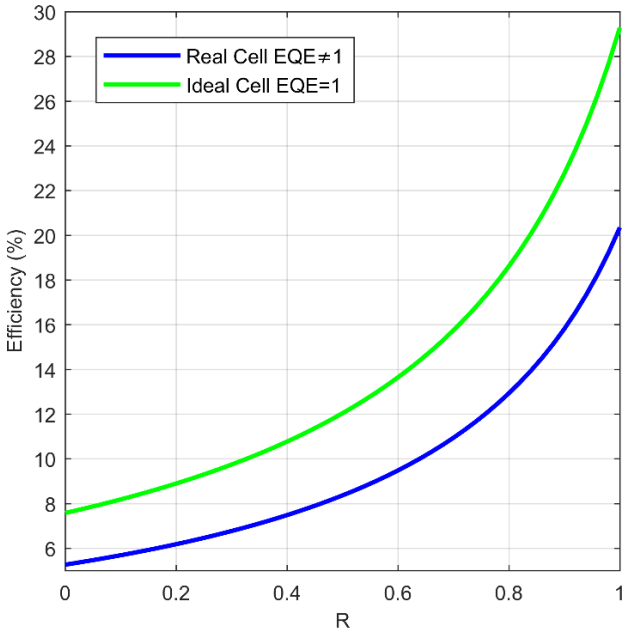

FIGURE 10. Comparison of the relationship between efficiency η (%) and BSR reflectivity R for an ideal TPV module (EQE = 1) and a real TPV module (EQE ≠ 1) at an average emitter temperature T of 1750K.

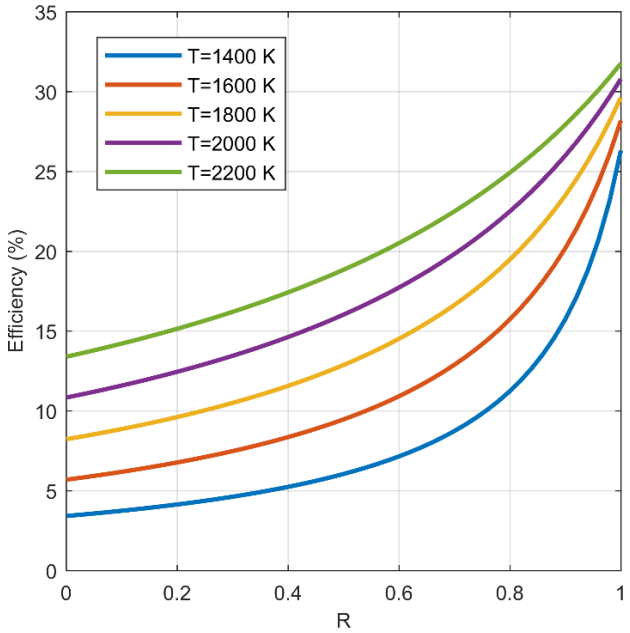

FIGURE 11. Effect of varying emitter temperature T on TPV conversion efficiency for a 0.25 cm^2 TPV module with EQE = 1. Increasing the emitter temperature increases the TPV conversion efficiency.

the photocurrent density I_{ph} is equal to 8.158 A/cm^2; I_L is 2.040 A; V_{oc} is equal to 0.5233 V; and V_m is 0.447 V. The efficiencies of real and ideal TPV modules are compared in Fig. 10 for an average T of 1750 K.

Fig. 10 shows the existing room for improvement in a real TPV module, as an ideal 0.25 cm^2 InGaAs TPV cell (EQE = 1) can attain efficiency as high as 29%, in contrast to 20% efficiency of a real TPV cell (average EQE = 0.7097), at the maximum BSR reflectivity of 1. The increase in efficiency is because, at higher EQE, the reflection, absorption, and recombination losses are a minimum.

The effect of varying emitter temperature on the efficiency of an ideal TPV cell (EQE = 1) with respect to BSR reflectivity is also analyzed in Fig. 11.

Fig. 11 is compared with Fig. 9, to determine the impact of varying the temperature of emitter for an ideal (EQE = 1) and real (EQE ≠ 1) TPV cell, respectively. The efficiency of an ideal cell with EQE = 1 also follows a trend like that followed when EQE ≠ 1, when the temperature is varied. However, overall, when EQE = 1 the efficiency values are much more competitive; at the graphite emitter temperature of 2200 K, when EQE = 1, the efficiency is equal to 31.75%, in contrast to 22.16% when EQE ≠ 1. $\eta \geq 30\%$ is a range that makes TPV solid-state engines competitive to turbines working on Rankine or Brayton Cycle.

E. COMPARISON OF THE EFFICIENCY ENHANCEMENT ACHIEVED IN THIS PAPER WITH RESULTS OF PREVIOUS CASE STUDIES WITH DIFFERENT EFFICIENCY ENHANCEMENT METHODS

Table 2 compares the significant results of the efficiency enhancement techniques investigated in this paper to the results that have been achieved by other authors for different techniques. In this paper, it was found that an emitter temperature of at least 1800 K is required to exceed the 20% efficiency threshold. However, for the purpose of comparison, the techniques studied in this paper such as BSR reflectivity and EQE, and those in other papers such as the use of multijunction cells in place of single junction cells, use of spectrally selective emitters, and different configurations and cavity arrangements of the TPV system have been tabulated and compared at the same emitter temperature of ∼1600 K. As per the existing work of other authors, the use of selective emitters [22] ($\eta = 8\%$ at $T = 1640$ K) and cylindrical cavities [77] ($\eta = 4.5\%$) have not yet been experimentally shown to attain high efficiencies.

V. CONCLUSION

In this work, the design parameters and configuration of a practical application of thermal engineering: a TPV system that is to be used in a CSP plant, is presented. The factors affecting the choice of material of a TPV cell are different from those of a conventional solar PV cell due to lower (< 2500 K) emitter temperatures. It is found that silicon (Si), despite being the most preferred solar cell material, is not suitable for TPV applications, as is shown by a small above-bandgap region of the cell on a Planck distribution curve of the emitter. Cells with moderate bandgap energy, Ge (0.66 eV), GaSb (0.72 eV), and InGaAs (0.74 eV), are the most favorable choices due to their low recombination rates, high above-bandgap region, and small difference between peak and bandgap wavelengths leading to smaller thermalization losses.

A CSP system with a TPV power cycle was modeled based on a hexagonal TPV cavity design. The significance of Back Surface Reflectors (BSR) in TPV systems was highlighted, as it was found that including a high reflectivity BSR ($R = 1$) alone (e.g. mirror), without any other changes in the system, can result in an efficiency increase of almost 15% for an InGaAs cell. It has been determined that increasing the emitter temperature also increases the efficiency of the TPV systems. For a real cell, with EQE < 1 varying with wavelength, the emitter temperatures must be kept at least above 1800 K, to have an efficiency exceeding 20%.

Lastly, the scope of future work was assessed by observing the surge in efficiency values caused by the usage of ideal TPV cells with an EQE of 1. Using multijunction cells, antireflection coatings, front surface texturing, and cells made of quantum nanostructures can improve the EQE of the cell and lead to an increase of almost 10% in efficiency values of a TPV module integrated with a BSR. The highest efficiency recorded in this analysis, with the inclusion of series resistance and dark current losses but exclusion of reflection and transmission losses (EQE = 1), was 31.75 %, for an emitter temperature of 2200 K and a BSR reflectivity of 1. This efficiency of 31.75% exceeds the efficiency of most turbines running on Rankine or Brayton cycle (30%), and the highest measured (to date) TPV conversion efficiency (29.1%) [28]. Among the suggested changes, the incorporation of a mirror as the BSR is the simplest of changes which must be introduced in all TPV systems. Thus, with improved research efforts in TPV technology, the compact TPV systems can replace turbines in CSP plants.

ACKNOWLEDGMENT

(Mohsina Asif, Khujista Nadeem, and Zertasha Shoukat contributed equally to this work.)

REFERENCES

[1] E. D. Coyle and R. A. Simmons, *Understanding the Global Energy Crisis*. West Lafayette, IN, USA: Purdue Univ. Press, 2014.

[2] M. Höök and X. Tang, "Depletion of fossil fuels and anthropogenic climate change—A review," *Energy Policy*, vol. 52, pp. 797–809, Jan. 2013.

[3] A. Cherp, V. Vinichenko, J. Jewell, M. Suzuki, and M. Antal, "Comparing electricity transitions: A historical analysis of nuclear, wind and solar power in Germany and Japan," *Energy Policy*, vol. 101, pp. 612–628, Feb. 2017.

[4] C. Zou, Q. Zhao, G. Zhang, and B. Xiong, "Energy revolution: From a fossil energy era to a new energy era," *Natural Gas Ind. B*, vol. 3, no. 1, pp. 1–11, Jan. 2016.

[5] K. Hansen, C. Breyer, and H. Lund, "Status and perspectives on 100% renewable energy systems," *Energy*, vol. 175, pp. 471–480, May 2019.

[6] T. Güney, "Renewable energy, non-renewable energy and sustainable development," *Int. J. Sustain. Develop. World Ecol.*, vol. 26, no. 5, pp. 389–397, Jul. 2019.

[7] F. Rizzi, N. J. van Eck, and M. Frey, "The production of scientific knowledge on renewable energies: Worldwide trends, dynamics and challenges and implications for management," *Renew. Energy*, vol. 62, pp. 657–671, Feb. 2014.

[8] M. Romero and A. Steinfeld, "Concentrating solar thermal power and thermochemical fuels," *Energy Environ. Sci.*, vol. 5, no. 11, pp. 9234–9245, 2012, doi: 10.1039/C2EE21275G.

[9] C. Hank, A. Sternberg, N. Köppel, M. Holst, T. Smolinka, A. Schaadt, C. Hebling, and H.-M. Henning, "Energy efficiency and economic assessment of imported energy carriers based on renewable electricity," *Sustain. Energy Fuels*, vol. 4, no. 5, pp. 2256–2273, May 2020, doi: 10.1039/D0SE00067A.

[10] D. Gielen, F. Boshell, D. Saygin, M. D. Bazilian, N. Wagner, and R. Gorini, "The role of renewable energy in the global energy transformation," *Energy Strategy Rev.*, vol. 24, pp. 38–50, Apr. 2019.

[11] E. L. Warren, M. G. Deceglie, M. Rienäcker, R. Peibst, A. C. Tamboli, and P. Stradins, "Maximizing tandem solar cell power extraction using a three-terminal design," *Sustain. Energy Fuels*, vol. 2, no. 6, pp. 1141–1147, 2018, doi: 10.1039/C8SE00133B.

[12] J. Barber, "Hydrogen derived from water as a sustainable solar fuel: Learning from biology," *Sustain. Energy Fuels*, vol. 2, no. 5, pp. 927–935, 2018, doi: 10.1039/C8SE00002F.

[13] K. W. Jung, M. R. Sohn, H. M. Lee, I. S. Yang, S. D. Sung, J. Kim, E. W.-G. Diau, and W. I. Lee, "Silver bismuth iodides in various compositions as potential Pb-free light absorbers for hybrid solar cells," *Sustain. Energy Fuels*, vol. 2, no. 1, pp. 294–302, 2018, doi: 10.1039/C7SE00477J.

[14] P. Cendula, M. T. Mayer, J. Luo, and M. Grätzel, "Elucidation of photovoltage origin and charge transport in Cu_2O heterojunctions for solar energy conversion," *Sustain. Energy Fuels*, vol. 3, no. 10, pp. 2633–2641, Sep. 2019, doi: 10.1039/C9SE00385A.

[15] R. S. Tuley, J. M. S. Orr, R. J. Nicholas, D. C. Rogers, P. J. Cannard, and S. Dosanjh, "Lattice-matched InGaAs on InP thermophovoltaic cells," *Semicond. Sci. Technol.*, vol. 28, no. 1, Jan. 2013, Art. no. 015013.

[16] E. Dahlquist, B. Karlsson, and E. Lindberg. (2011). *Combined Solar Power and TPV*. [Online]. Available: https://www.ep.liu.se/ecp/057/vol11/003/ecp57vol11_003.pdf

[17] S. V. Boriskina, J. K. Tong, V. Ferry, J. Michel, and A. Kildishev, "Breaking the limits of optical energy conversion," *Opt. Photon. News*, vol. 26, no. 7, pp. 48–51, 2015.

[18] H. R. Seyf and A. Henry, "Thermophotovoltaics: A potential pathway to high efficiency concentrated solar power," *Energy Environ. Sci.*, vol. 9, no. 8, pp. 2654–2665, 2016.

[19] A. McClelland and M. Mankin, *Optical Measurements for Scientists and Engineers: A Practical Guide*. Cambridge, U.K.: Cambridge Univ. Press, 2018.

[20] T. Bauer, *Thermophotovoltaics: Basic Principles and Critical Aspects of System Design*. Stuttgart, Germany: Springer, 2011.

[21] A. Yuksel, A. Heltzel, and J. R. Howell, "Design and optimization of thermal selective emitters for high-efficiency thermophotovoltaic (TPV) power generation," in *Proc. Energy Sustainability*. New York, NY, USA: American Society Mechanical Engineers, vol. 56840, 2015, Art. no. V001T10A003.

[22] N. A. Pfiester and T. E. Vandervelde, "Selective emitters for thermophotovoltaic applications," *Phys. Status Solidi A*, vol. 214, no. 1, Jan. 2017, Art. no. 1600410, doi: 10.1002/pssa.201600410.

[23] A. Belghachi, "Theoretical calculation of the efficiency limit for solar cells," in *Solar Cells: New Approaches and Reviews*. Rijeka, Croatia: InTech, 2015.

[24] D. Jiang, W. Yang, K. J. Chua, and J. Ouyang, "Thermal performance of micro-combustors with baffles for thermophotovoltaic system," *Appl. Thermal Eng.*, vol. 61, no. 2, pp. 670–677, Nov. 2013.

[25] S. Bani, J. Pan, A. Tang, Q. Lu, and Y. Zhang, "Micro combustion in a porous media for thermophotovoltaic power generation," *Appl. Thermal Eng.*, vol. 129, pp. 596–605, Jan. 2018.

[26] C.-C. Chang, W. J. M. Kort-Kamp, J. Nogan, T. S. Luk, A. K. Azad, A. J. Taylor, D. A. R. Dalvit, M. Sykora, and H.-T. Chen, "High-temperature refractory metasurfaces for solar thermophotovoltaic energy harvesting," *Nano Lett.*, vol. 18, no. 12, pp. 7665–7673, Dec. 2018.

[27] H. Wang, J.-Y. Chang, Y. Yang, and L. Wang, "Performance analysis of solar thermophotovoltaic conversion enhanced by selective metamaterial absorbers and emitters," *Int. J. Heat Mass Transf.*, vol. 98, pp. 788–798, Jul. 2016.

[28] Z. Omair, G. Scranton, L. M. Pazos-Outón, T. P. Xiao, M. A. Steiner, V. Ganapati, P. F. Peterson, J. Holzrichter, H. Atwater, and E. Yablonovitch, "Ultraefficient thermophotovoltaic power conversion by band-edge spectral filtering," *Proc. Nat. Acad. Sci. USA*, vol. 116, no. 31, pp. 15356–15361, Jul. 2019.

[29] A. Datas, "Optimum semiconductor bandgaps in single junction and multijunction thermophotovoltaic converters," *Sol. Energy Mater. Sol. Cells*, vol. 134, pp. 275–290, Mar. 2015, doi: 10.1016/j.solmat.2014.11.049.

[30] H. H. Kolm, "Quarterly progress report, solid state research, group 35," MIT-Lincoln Lab., Lexington, MA, USA, vol. 1, May 1956.
[31] G. G. Pethuraja, R. E. Welser, A. K. Sood, C. Lee, N. J. Alexander, H. Efstathiadis, P. Haldar, and J. L. Harvey, "Effect of Ge incorporation on bandgap and photosensitivity of amorphous SiGe thin films," *Mater. Sci. Appl.*, vol. 3, no. 2, 2012, Art. no. 17248. [Online]. Available: http://www.scirp.org/journal/paperinformation.aspx?paperid=17248
[32] L. Tang, J. D. MacKenzie, J. E. Avery, and L. M. Fraas, "Low cost GaSb n on p ThermoPhotoVoltaic (TPV) cells," in *Proc. IEEE 46th Photovolt. Spec. Conf. (PVSC)*, Jun. 2019, pp. 0230–0232.
[33] A. Cabrera, A. Ramos, I. Artacho, M. Gomez, K. Gavin, A. Marti, and A. Datas, "Thermophotovoltaic efficiency measurement: Design and analysis of a novel experimental method," in *Proc. Spanish Conf. Electron Devices (CDE)*, Nov. 2018, pp. 1–4.
[34] T. Buonassisi, "2.627 fundamentals of photovoltaics," Massachusetts Inst. Technol., Cambridge, MA, USA, MIT OpenCourseWare, Fall 2013. [Online]. Available: https://ocw.mit.edu
[35] H. Heidarzadeh, A. Rostami, and M. Dolatyari, "Management of losses (thermalization-transmission) in the Si-QDs inside 3C–SiC to design an ultra-high-efficiency solar cell," *Mater. Sci. Semicond. Process.*, vol. 109, Apr. 2020, Art. no. 104936.
[36] J. Guillemoles, "Future concepts for photovoltaic energy conversion," in *Fundamentals of Materials for Energy and Environmental Sustainability*, vol. 238. Cambridge, U.K.: Cambridge Univ. Press, 2011.
[37] M. P. Bernardi, O. Dupré, E. Blandre, P.-O. Chapuis, R. Vaillon, and M. Francoeur, "Impacts of propagating, frustrated and surface modes on radiative, electrical and thermal losses in nanoscale-gap thermophotovoltaic power generators," *Sci. Rep.*, vol. 5, no. 1, pp. 1–12, Dec. 2015.
[38] R. Nicholas and R. Tuley, "Thermophotovoltaic (TPV) devices: Introduction and modelling," in *Functional Materials for Sustainable Energy Applications*. Amsterdam, The Netherlands: Elsevier, 2012, pp. 67–90.
[39] Y. Wang, H. Liu, and J. Zhu, "Solar thermophotovoltaics: Progress, challenges, and opportunities," *APL Mater.*, vol. 7, no. 8, Aug. 2019, Art. no. 080906.
[40] L. Yu and A. Zunger, "Identification of potential photovoltaic absorbers based on first-principles spectroscopic screening of materials," *Phys. Rev. Lett.*, vol. 108, no. 6, Feb. 2012, Art. no. 068701.
[41] A. G. Atkins, T. Atkins, and M. Escudier, *A Dictionary of Mechanical Engineering*. Oxford, U.K.: Oxford Univ. Press, 2013.
[42] H. Wang, H. Ye, and Y. Zhang, "Preparation and performance evaluation of Er_2O_3 coating-type selective emitter," *Sci. China Technol. Sci.*, vol. 57, no. 2, pp. 332–338, Feb. 2014.
[43] J.-M. Kim, K.-H. Park, D.-S. Kim, B.-Y. Hwang, S.-K. Kim, H.-M. Chae, B.-K. Ju, and Y.-S. Kim, "Design and fabrication of spectrally selective emitter for thermophotovoltaic system by using nano-imprint lithography," *Appl. Surf. Sci.*, vol. 429, pp. 138–143, Jan. 2018.
[44] E. S. Sakr, Z. Zhou, and P. Bermel, "High efficiency rare-Earth emitter for thermophotovoltaic applications," *Appl. Phys. Lett.*, vol. 105, no. 11, Sep. 2014, Art. no. 111107.
[45] Z. Zhou, O. Yehia, and P. Bermel, "Integrated photonic crystal selective emitter for thermophotovoltaics," *J. Nanophotonics*, vol. 10, no. 1, Mar. 2016, Art. no. 016014.
[46] Z. Utlu and B. S. Önal, "Thermodynamic analysis of thermophotovoltaic systems used in waste heat recovery systems: An application," *Int. J. Low-Carbon Technol.*, vol. 13, no. 1, pp. 52–60, Mar. 2018.
[47] A. Karalis and J. D. Joannopoulos, "Transparent and 'opaque'conducting electrodes for ultra-thin highly-efficient near-field thermophotovoltaic cells," *Sci. Rep.*, vol. 7, no. 1, pp. 1–11, Dec. 2017.
[48] C. Amy, H. R. Seyf, M. A. Steiner, D. J. Friedman, and A. Henry, "Thermal energy grid storage using multi-junction photovoltaics," *Energy Environ. Sci.*, vol. 12, no. 1, pp. 334–343, 2019.
[49] G. Scranton, T. P. Xiao, V. Ganapati, J. Holzrichter, P. F. Peterson, and E. Yablonovitch, "Highly efficient thermophotovoltaics enabled by photon re-use," in *Proc. IEEE 43rd Photovolt. Spec. Conf. (PVSC)*, Jun. 2016, pp. 1026–1029.
[50] T. L. Bergman, F. P. Incropera, D. P. DeWitt, and A. S. Lavine, *Fundamentals of Heat and Mass Transfer*. Hoboken, NJ, USA: Wiley, 2011.
[51] N. A. Pfiester, D. F. DeMeo, C. Shemela, and T. Vandervelde, "Thermophotovoltaic efficiency enhancement through metamaterial selective emitters," in *Proc. 28th Eur. Photovolt. Sol. Energy Conf. Exhib.*, 2013, pp. 269–273.
[52] P. Kiameh, *Power Generation Handbook 2/E*. New York, NY, USA: McGraw-Hill Education, 2011.
[53] F. Bouzid and L. Dehimi, "Performance evaluation of a GaSb thermophotovoltaic converter," *Revue des Énergies Renouvelables*, vol. 15, no. 3, pp. 383–397, 2012.
[54] C. Ferrari, F. Melino, M. Pinelli, P. R. Spina, and M. Venturini, "Overview and status of thermophotovoltaic systems," *Energy Procedia*, vol. 45, pp. 160–169, Jan. 2014.
[55] W. Shockley and H. J. Queisser, "Detailed balance limit of efficiency of p-n junction solar cells," *J. Appl. Phys.*, vol. 32, no. 3, pp. 510–519, 1961.
[56] L. M. Fraas and L. D. Partain, *Solar Cells and Their Applications*. Hoboken, NJ, USA: Wiley, 2010.
[57] R. Bhatt, I. Kravchenko, and M. Gupta, "High-efficiency solar thermophotovoltaic system using a nanostructure-based selective emitter," *Sol. Energy*, vol. 197, pp. 538–545, Feb. 2020.
[58] N. M. A. Alrahim Shannan, N. Z. Yahaya, and B. Singh, "Single-diode model and two-diode model of PV modules: A comparison," in *Proc. IEEE Int. Conf. Control Syst., Comput. Eng.*, Nov. 2013, pp. 210–214.
[59] D. Jena and V. V. Ramana, "Modeling of photovoltaic system for uniform and non-uniform irradiance: A critical review," *Renew. Sustain. Energy Rev.*, vol. 52, pp. 400–417, Dec. 2015.
[60] M. Hejri, H. Mokhtari, M. R. Azizian, M. Ghandhari, and L. Soder, "On the parameter extraction of a five-parameter double-diode model of photovoltaic cells and modules," *IEEE J. Photovolt.*, vol. 4, no. 3, pp. 915–923, May 2014.
[61] S. Rißland and O. Breitenstein, "Considering the distributed series resistance in a two-diode model," *Energy Procedia*, vol. 38, pp. 167–175, Sep. 2013.
[62] O. Breitenstein and S. Rißland, "A two-diode model regarding the distributed series resistance," *Sol. Energy Mater. Sol. Cells*, vol. 110, pp. 77–86, Mar. 2013.
[63] C. Honsberg and S. Bowden. (2019). *Double Diode Model: PV Education*. [Online]. Available: https://www.pveducation.org/pvcdrom/characterisation/double-diode-model
[64] M. Norton, A. M. G. Amillo, and R. Galleano, "Comparison of solar spectral irradiance measurements using the average photon energy parameter," *Sol. Energy*, vol. 120, pp. 337–344, Oct. 2015, doi: 10.1016/j.solener.2015.06.023.
[65] E. L. Meyer, "Extraction of saturation current and ideality factor from measuring V_{oc} and I_{sc} of photovoltaic modules," *Int. J. Photoenergy*, vol. 2017, pp. 1–9, Dec. 2017.
[66] J. Cubas, S. Pindado, and F. Sorribes-Palmer, "Analytical calculation of photovoltaic systems maximum power point (MPP) based on the operation point," *Appl. Sci.*, vol. 7, no. 9, p. 870, Aug. 2017.
[67] M. A. Green, K. Emery, D. L. King, S. Igari, and W. Warta, "Solar cell efficiency tables (version 22)," *Prog. Photovolt., Res. Appl.*, vol. 11, no. 5, pp. 347–352, 2003.
[68] A. Lenert, D. M. Bierman, Y. Nam, W. R. Chan, I. Celanovic, M. Soljacic, and E. N. Wang, "A nanophotonic solar thermophotovoltaic device," *Nature Nanotechnol.*, vol. 9, no. 2, pp. 126–130, Feb. 2014.
[69] T. Saga, "Advances in crystalline silicon solar cell technology for industrial mass production," *NPG Asia Mater.*, vol. 2, no. 3, pp. 96–102, Jul. 2010.
[70] R. S. Tuley and R. J. Nicholas, "Band gap dependent thermophotovoltaic device performance using the InGaAs and InGaAsP material system," *J. Appl. Phys.*, vol. 108, no. 8, Oct. 2010, Art. no. 084516.
[71] J. K. Tong, W.-C. Hsu, Y. Huang, S. V. Boriskina, and G. Chen, "Thin-film 'thermal well' emitters and absorbers for high-efficiency thermophotovoltaics," *Sci. Rep.*, vol. 5, no. 1, p. 10661, Sep. 2015, doi: 10.1038/srep10661.
[72] M. Chakraburtty, "IV-VI materials & devices for thermophotovoltaic (TPV) power generation," M.S. thesis, Univ. Oklahoma, Norman, OK, USA, 2016.
[73] J. Wang, J. Zhang, Y. Zhou, H. Liu, Q. Xue, X. Li, C.-C. Chueh, H.-L. Yip, Z. Zhu, and A. K. Y. Jen, "Highly efficient all-inorganic perovskite solar cells with suppressed non-radiative recombination by a Lewis base," *Nature Commun.*, vol. 11, no. 1, pp. 1–9, Dec. 2020.
[74] M. K. Ray, S. Sasmal, and S. Maity, "Improvement of quantum efficiency and reflectance of GaAs solar cell," *Int. J. Eng. Res. Gen. Sci.*, vol. 3, no. 2, Mar./Apr. 2015.
[75] F. Bendelala, A. Cheknane, and H. Hilal, "Enhanced low-gap thermophotovoltaic cell efficiency for a wide temperature range based on a selective meta-material emitter," *Sol. Energy*, vol. 174, pp. 1053–1057, Nov. 2018.

[76] A. Datas and A. Martí, "Thermophotovoltaic energy in space applications: Review and future potential," *Sol. Energy Mater. Sol. Cells*, vol. 161, pp. 285–296, Mar. 2017.
[77] V. P. Khvostikov, S. V. Sorokina, N. S. Potapovich, O. A. Khvostikova, A. V. Malievskaya, A. S. Vlasov, M. Z. Shvarts, N. K. Timoshina, and V. M. Andreev, "Thermophotovoltaic generators based on gallium antimonide," *Semiconductors*, vol. 44, no. 2, pp. 255–262, Feb. 2010.

ALI H. KAZIM received the Ph.D. degree from the Georgia Institute of Technology, USA. He was a Visiting Researcher at The University of Texas at Dallas, USA. He is currently serving as an Assistant Professor with the Department of Mechanical Engineering, University of Engineering and Technology Lahore, Lahore, Pakistan. He is also the Director of the Heat Transfer Laboratory. His current research interests include thermophotovoltaics, diesel engines, thermal properties, solar radiation management, and thermoelectrics.

MOHSINA ASIF received the B.Sc. degree in mechanical engineering from the University of Engineering and Technology Lahore, Lahore, Pakistan.

She has also conducted research on sustainable HVAC systems and the effects of ambient weather conditions on the performance of solar PV modules.

KHUJISTA NADEEM received the B.S. degree in mechanical engineering from the University of Engineering and Technology Lahore, Lahore, Pakistan.

She served as an Intern at SUPARCO-SRDC, Lahore, in the summer of 2019, where she studied the trends in satellite and solar module manufacturers and analyzed national satellites already placed in orbit. She has also worked on the weather conditions affecting solar cells.

ZERTASHA SHOUKAT received the B.S. degree in mechanical engineering from the University of Engineering and Technology Lahore, Lahore, Pakistan.

She has also worked on the effects of temperature and wind speed on the efficiency of the PV module.

RABIA NAZIR (Member, IEEE) received the Ph.D. degree from the University of Canterbury, New Zealand. She is currently serving as an Assistant Professor with the University of Engineering and Technology Lahore. Her current research interests include smart grid technologies, power converter design, implementations, and control, and renewable and distributed generation technologies.

MUHAMMAD SOHAIL MALIK (Senior Member, IEEE) received the Ph.D. degree from the Universita Politecnica delle Marche, Italy. He is currently an Assistant Professor with the Faculty of Mechanical Engineering, Ghulam Ishaq Khan Institute of Engineering Sciences and Technology, Pakistan. Being a Senior Member of the IEEE, he has a combined experience of academia and industry of about 15 years. He has worked in the areas of energy management, energy harvesting, composite materials, and opto-acoustic non-destructive testing. While extending his core expertise of applied finite-element analysis, his current research interests include multi body dynamics and applications of UAVs.

AQSA SHABBIR received the joint Ph.D. degree from Ghent University, Belgium, and from the Ludwig-Maximillian University of Munich, Germany. She was a Visiting Researcher with the Max Planck Institute for Plasma Physics, Garching, Germany, and the Culham Centre for Fusion Energy, U.K. She is currently an Associate Professor with the Department of Electrical Engineering, Lahore College for Women University. Her current research interests include pattern recognition, machine learning, advanced data analysis for nuclear fusion, power electronics, and renewable energy generation.